Geometrical optics approach in liquid crystal films with three-dimensional director variations

G. Panasyuk,[1] J. Kelly,[2] E. C. Gartland,[3] and D. W. Allender[1]
[1]*Department of Physics, Kent State University, Kent, Ohio 44242*
[2]*Liquid Crystal Institute, Kent State University, Kent, Ohio 44242*
[3]*Department of Mathematical Sciences, Kent State University, Kent, Ohio 44242*
(Received 9 October 2002; published 10 April 2003)

A formal geometrical optics approach (GOA) to the optics of nematic liquid crystals whose optic axis (director) varies in more than one dimension is described. The GOA is applied to the propagation of light through liquid crystal films whose director varies in three spatial dimensions. As an example, the GOA is applied to the calculation of light transmittance for the case of a liquid crystal cell which exhibits the homeotropic to multidomainlike transition (HMD cell). Properties of the GOA solution are explored, and comparison with the Jones calculus solution is also made. For variations on a smaller scale, where the Jones calculus breaks down, the GOA provides a fast, accurate method for calculating light transmittance. The results of light transmittance calculations for the HMD cell based on the director patterns provided by two methods, direct computer calculation and a previously developed simplified model, are in good agreement.

DOI: 10.1103/PhysRevE.67.041702 PACS number(s): 61.30.Cz, 78.20.Bh

I. INTRODUCTION

Optics is one of the primary empirical tools for investigating the physical behavior of liquid crystals. Optical measurements can be used to infer director orientation, identify phases, and study the dynamics of director fluctuations. In addition, the optical behavior of liquid crystals is of technological importance because of the use of liquid crystals in display applications. As the physics and technology of liquid crystals advance, there is a need for better understanding of the optics at smaller and smaller feature sizes. The study of defect structures and confinement of liquid crystals in micrometer-sized cavities are two examples of areas of active research. At the same time, microdisplays and switchable diffractive elements for optical communications have pushed applied research on liquid crystals into the micrometer regime.

There have been several approaches to handling multidimensional optics calculations for liquid crystals. The simplest involves extending one-dimensional techniques such as the 4×4 matrix methods [1] or the Jones calculus [2]. In these approaches, the liquid crystal is treated locally as having index variations only along the direction of light propagation: lateral variations in optical properties are ignored [3]. The multidimensional behavior is then obtained as a composite of several one-dimensional calculations. This simple description should be applicable when the wavelength of light λ is very small relative to the liquid crystal feature sizes of interest.

At the other extreme, when the feature sizes are smaller than λ, a direct solution of Maxwell's equations is required. Because of the complexity of any physically interesting problem, no analytical solutions are possible, and computer calculations are necessary. In this regard, the so-called finite difference time domain (FDTD) method has been the most widely used [4–8]. Later, Kriezis and Elston introduced a wide-angle beam propagation method (BPM) for two-dimensional liquid crystal optics problems [9–11]. In [9,10], their development had the following restrictions: the director must lie in a plane, and that plane must be the plane of incidence; reflections must be minimal. Within these bounds, however, they demonstrated that the results of the BPM are in excellent agreement with FDTD calculations even when the geometry is comparable in size to λ. Furthermore, the technique is very amenable to numerical calculation, being stable and fast compared to the FDTD approach. Later, in [11], Kriezis and Elston generalized the proposed method to handle a liquid crystal (LC) cell with a tilted-twisted director profile, considering a light-wave propagation in a twisted nematic microdisplay pixel. Again, it has been shown that in its regime of validity the BPM can reproduce FDTD simulations with good accuracy.

In this paper another description of the multidimensional optics of liquid crystal media is considered, the geometrical optics approach (GOA), which bridges the gap between these two regimes. As is known, the GOA is applicable if the parameter $\kappa=1/k_0 l$ is small. Here l is the characteristic scale of the medium inhomogeneity, $k_0=2\pi/\lambda$, and λ is the vacuum wavelength. In an anisotropic medium, which can be characterized in our case by the dielectric tensor $\hat{\epsilon}$ (we consider a liquid crystal material without absorption or spatial dispersion, whose magnetic permeability is equal to 1). The strength of the anisotropy can be described by the parameter $\nu=\max|\epsilon_{ik}-\epsilon_0\delta_{ik}|$, where $\epsilon_0=\frac{1}{3}\mathrm{Tr}\,\hat{\epsilon}$. There is a substantial literature on the GOA for isotropic media, where $\nu=0$ (see, for example, [12] and references there), on the one hand, and, on the other hand, for anisotropic media with relatively high birefringence, when $\nu\gg\kappa$ [12–14]. In the latter case the normal waves (ordinary and extraordinary waves in our problems) can be treated independently (the Courant-Lax method), and interaction between them is negligible. A reasonable and useful approach for studying wave propagation through a medium with ''weak'' anisotropy, when ν is of the order of κ (or $\nu<\kappa$), was proposed and developed in [15,16]. It was shown that in a region of weak birefringence a strong interaction between the normal modes occurs, which leads to a redistribution of energy between the normal waves. The basic assumption of this ''quasi-isotropic approach,'' described in detail in [16], is to use the isotropic form of geometrical optics equations as the zeroth approximation, and

then to consider the anisotropy tensor $\nu_{ik}=\epsilon_{ik}-\epsilon_0\delta_{ik}$ as a perturbation of the same order of magnitude as κ. The ray path technique has also been employed in these studies. In accordance with this technique, one determines first the ray trajectories together with the local wave vectors $\mathbf{k}(\mathbf{r})$ along them, and, in the next stage, one determines the amplitudes of normal waves along the rays, using moving coordinate systems attached to each ray. The method developed was applied successfully to different problems, such as electromagnetic wave propagation in plasma (solar, ionospheric, laboratory) and optical and elastic phenomena in crystals and deformed isotropic media.

Ong and Meyer [17,18] and Ong [19,20] were the first to apply geometrical optics extensively to liquid crystals. They developed the theoretical framework for geometrical optics of liquid crystals in one dimension and applied the GOA to several basic and technological problems. Since then, the GOA has been applied to liquid crystal problems where the director varies in two dimensions, with the same restriction as mentioned above for the BPM: the director lies in a plane which is also the plane of incidence. These restrictions remove any coupling between the ordinary and extraordinary rays, permitting a ray tracing approach to geometrical optics. Kosmopoulos and Senginoglou [21,22] used the geometrical optics ray technique to study ray trajectories and intensity variations for light propagating through a periodically distorted homogeneous nematic layer. Later, Reyes [23] applied geometric optics to the multidimensional problem of a nematic liquid crystal confined in a spherical cavity. He studied the ray trajectories in the equatorial plane of a droplet with radial director configuration but did not explore the variations in field amplitude. Recently, Liu, Kelly, and Chen successfully applied the GOA to study the electro-optical performance of a self-compensating vertically aligned liquid crystal display cell [24], using a two-dimensional (2D) liquid crystal display mode which combines the concepts of the in-plane switching mode with vertical alignment [25,26]. In [27] the GOA coupled with Kirchhoff diffraction theory was applied to study optical properties of a switchable diffraction grating, where the same cell [25,26] was used. For this 2D cell it has also been shown that, for the conditions when the BPM is applicable, the GOA is in reasonable agreement with BPM (and FDTD) calculations even if l is comparable with λ. This contrasts with the Jones calculus, which differs significantly from the GOA, BPM, and FDTD results for l comparable with λ.

In our study we consider the GOA equations as partial differential equations which follow directly from the Maxwell equations when $\kappa \ll 1$. In our opinion, this way of finding the GOA solutions is more convenient than the ray path technique, because it employs a laboratory frame (convenient for the LC cell under consideration) without resorting to the curvilinear coordinate systems associated with rays, and a uniform mesh can be used. We do not consider the anisotropy of $\hat{\epsilon}$ as being small, and in the present study κ is the only small parameter. This is important because, even if $\nu \ll 1$, the relation $\nu \sim \kappa$ usually holds only in wall defect or near-substrate regions at a relatively high voltage. Outside these regions, however, $\nu \gg \kappa$, and the error related to neglecting contributions of the order of ν^2 could be larger than second order (and higher) geometrical optics corrections. In order to describe regions where $\nu \sim \kappa$, mode coupling between ordinary and extraordinary waves is introduced, although in a way different from the methods used in [16]. In Sec. II the mathematical formalism of the GOA in the case of a liquid crystal cell with a multidimensional director distribution is considered, and in Sec. III an application of the GOA to a cell with a three-dimensional director is described.

II. MATHEMATICAL ASPECTS OF THE GOA

The time-harmonic wave equation for the electric field is derived from Maxwell's equations and has the following form in a nonconductive dielectric medium:

$$\nabla^2\mathbf{E}-\boldsymbol{\nabla}(\boldsymbol{\nabla}\cdot\mathbf{E})=(ik_0)^2\hat{\epsilon}\mathbf{E}. \tag{1}$$

The GOA uses an expansion for the electric field $\mathbf{E}$ in powers of λ,

$$\mathbf{E}(\mathbf{r})=e^{ik_0S(\mathbf{r})}\sum_{m=0}^{\infty}\frac{\mathbf{E}_m(\mathbf{r})}{(ik_0)^m}, \tag{2}$$

and a similar expression for the magnetic field with the following substitution: $\mathbf{E}(\mathbf{r})\rightarrow\mathbf{H}(\mathbf{r})$ and $\mathbf{E}_m(\mathbf{r})\rightarrow\mathbf{H}_m(\mathbf{r})$. This expansion is well justified when λ is small relative to spatial variations of $\mathbf{E}_m$ and $\mathbf{H}_m$.

In Eq. (2) [and the corresponding expression for $\mathbf{H}_m(\mathbf{r})$], the function $S(\mathbf{r})$ is the optical path length or, as it is sometimes called, the eikonal. The surfaces of constant S are orthogonal to the local wave vector direction $[\mathbf{n}(\mathbf{r})\equiv\boldsymbol{\nabla}\mathbf{S}]$ and are the wave fronts of geometrical optics.

After substituting Eq. (2) into Eq. (1), the lowest order terms [of order $(ik_0)^2$] give the following equation:

$$[(\boldsymbol{\nabla}S)_i(\boldsymbol{\nabla}S)_k-(\boldsymbol{\nabla}S)^2\delta_{ik}+\epsilon_{ik}]E_{0k}=0 \tag{3}$$

(here and subsequently summing on repeated indices is assumed), which is equivalent to three homogeneous linear equations for the three components of $\mathbf{E}_0$. The compatability conditions of Eq. (3) demand that

$$\det|(\boldsymbol{\nabla}S)_i(\boldsymbol{\nabla}S)_k-(\boldsymbol{\nabla}S)^2\delta_{ik}+\epsilon_{ik}|=0. \tag{4}$$

If one denotes $n_i=(\boldsymbol{\nabla}S)_i$, Eq. (4) formally coincides with the well known Fresnel equation for the vector $\mathbf{n}=\mathbf{k}/k_0$, where $\mathbf{k}$ is the wave vector in the medium (see, for example, [28]). In our case, we have the following expression for the dielectric tensor ϵ_{ik} through the director $\hat{\mathbf{n}}$:

$$\epsilon_{ik}=n_o^2\delta_{ik}+\Delta\epsilon\hat{n}_i\hat{n}_k, \tag{5}$$

where $\Delta\epsilon=n_e^2-n_o^2$. Here n_o and n_e are the ordinary and extraordinary indices of refraction. Calculating the determinant in Eq. (4) in a local coordinate system where the uniaxial dielectric tensor is diagonal, one can rewrite Eq. (4) as

$$[(\boldsymbol{\nabla}S)^2-n_o^2][(\boldsymbol{\nabla}S)^2-n_{\mathrm{eff}}^2]=0. \tag{6}$$

Equation (6) is an eigenvalue equation with two nondegenerate eigenvectors. One solution, which we denote as **o**, corresponds to the ordinary wave, whose eigenvalue satisfies the characteristic equation

$$(\nabla S_o)^2 = n_o^2, \tag{7}$$

where S_o is the optical path length associated with this eigenmode. The second eigenvector, designated **e**, is the extraordinary wave with characteristic equation

$$(\nabla S_e)^2 = n_{\mathrm{eff}}^2. \tag{8}$$

The effective index of refraction in Eqs. (6) and (8) is defined by the following expression:

$$n_{\mathrm{eff}} = n_{\mathrm{eff}}(\alpha) = \frac{n_o n_e}{\sqrt{n_o^2 \sin^2(\alpha) + n_e^2 \cos^2(\alpha)}}, \tag{9}$$

where α is the angle between ∇S_e and the (local) optic axis. Unlike the case of homogeneous anisotropic media considered in [28], here the director $\hat{\mathbf{n}}$ (and hence the optical axis) is a function of the space coordinates **r**. This means that in our inhomogeneous case the right-hand side of Eq. (9) is also a function of ∇S_e and $\hat{\mathbf{n}}$, which makes Eq. (8) a complicated partial differential equation. For further consideration of Eq. (8), it is convenient to eliminate α from this equation using Eq. (9) and the relation

$$\cos^2(\alpha) = \frac{(\hat{\mathbf{n}} \cdot \nabla S_e)^2}{(\nabla S_e)^2}. \tag{10}$$

Substituting Eq. (10) into Eq. (9), one can rewrite Eq. (8) for the extraordinary eikonal in the following form:

$$(\nabla S_e)^2 + \Delta\hat{\epsilon}(\hat{\mathbf{n}} \cdot \nabla S_e)^2 = n_e^2 \tag{11}$$

with $\Delta\hat{\epsilon} \equiv \Delta\epsilon / n_o^2$. Because all the expressions in Eqs. (9) and (10) are scalars, one can consider Eq. (11) in a laboratory coordinate system.

Equation (11) can be rewritten as

$$A\left(\frac{\partial S_e}{\partial z}\right)^2 + 2B\frac{\partial S_e}{\partial z} - C = 0, \tag{12}$$

where the coefficients A, B, and C can be expressed through the director components and x and y derivatives of S_e in the following way:

$$A = 1 + \Delta\hat{\epsilon}\hat{n}_z^2, \tag{13}$$

$$B = \Delta\hat{\epsilon}\left[\hat{n}_x\frac{\partial S_e}{\partial x} + \hat{n}_y\frac{\partial S_e}{\partial y}\right], \tag{14}$$

$$C = n_e^2 - \left(\frac{\partial S_e}{\partial x}\right)^2 - \left(\frac{\partial S_e}{\partial y}\right)^2 - \Delta\hat{\epsilon}\left[\hat{n}_x\frac{\partial S_e}{\partial x} + \hat{n}_y\frac{\partial S_e}{\partial y}\right]^2. \tag{15}$$

Assume that light propagates in some direction in the half space of increasing z coordinate. Equation (12) gives

$$\frac{\partial S_e}{\partial z} = \frac{-B \pm \sqrt{B^2 + AC}}{A}, \tag{16}$$

where the plus sign describes the forward propagating wave and the negative sign stands for the reflected wave. In what follows, reflections are ignored. Equations (7) and (16) must be solved with appropriate boundary conditions which depend on the properties of the liquid crystal cell and the properties of the isotropic medium adjacent to the cell. A particular example of a 3D liquid crystal cell is considered in Sec. III.

If S_o and S_e are known, Eq. (3) allows one to obtain also the directions of the electric vectors of the ordinary **o** and extraordinary **e** waves. Substituting $S = S_o$ into Eq. (3) gives the following system of equations to determine $\mathbf{E}_0 = \mathbf{o} \equiv (o_x, o_y, o_z)$:

$$c_{ik}^{(o)} o_k = 0, \tag{17}$$

where

$$c_{ik}^{(o)} = (\nabla S_o)_i (\nabla S_o)_k + \Delta\epsilon\hat{n}_i\hat{n}_k. \tag{18}$$

Because the determinant of this system is zero, two components of the vector **o** can be expressed through the third one, and one finds

$$\mathbf{o} = \gamma(N_{yz}\hat{x} + N_{zx}\hat{y} + N_{xy}\hat{z}). \tag{19}$$

Here $\hat{x}$, $\hat{y}$, and $\hat{z}$ are the unit vectors of the laboratory frame, and

$$(N_{yz}\hat{\mathbf{x}} + N_{zx}\hat{\mathbf{y}} + N_{xy}\hat{\mathbf{z}}) \equiv \mathbf{N} = \hat{\mathbf{n}} \times \nabla S_o. \tag{20}$$

The coefficient of proportionality γ in Eq. (19) is not unique. A possible choice for γ is $\gamma = (N_{yz}^2 + N_{zx}^2 + N_{xy}^2)^{-1/2}$, which makes the vector **o** a unit vector. In the same way, substituting $S = S_e$ into Eq. (3) produces a similar system of equations to determine the extraordinary electric vector $\mathbf{E}_0 = \mathbf{e} \equiv (e_x, e_y, e_z)$:

$$[c_{ik}^{(e)} - \delta n_e \delta_{ik}] e_k = 0, \tag{21}$$

where

$$c_{ik}^{(e)} = (\nabla S_e)_i (\nabla S_e)_k + \Delta\epsilon\hat{n}_i\hat{n}_k$$

and

$$\delta n_e = [(\nabla S_e)^2 - n_o^2]. \tag{22}$$

Using Eq. (11) for the extraordinary eikonal, one can express $(\hat{\mathbf{n}} \cdot \nabla S_e)^2$ through δn_e:

$$(\hat{\mathbf{n}} \cdot \nabla S_e)^2 = n_o^2\left(1 - \frac{1}{\Delta\epsilon}\right)\delta n_e. \tag{23}$$

On the other hand, a straightforward calculation shows that $(\hat{\mathbf{n}} \times \nabla S_e)^2 = (\nabla S_e)^2 - (\hat{\mathbf{n}} \cdot \nabla S_e)^2$, which allows one eventually to find δn_e as

$$\delta n_e = \frac{\Delta\epsilon}{n_e^2}(\mathbf{N}_e)^2 \tag{24}$$

with

$$\mathbf{N}_e \equiv \hat{\mathbf{n}} \times \boldsymbol{\nabla} S_e = N_{yz}^e \hat{x} + N_{zx}^e \hat{y} + N_{xy}^e \hat{z}. \tag{25}$$

As in the ordinary case, the determinant of the system (21) is zero, and one can express again two components of the vector **e** through the third one. Using also the relation (24), one finds that

$$\mathbf{e} = \gamma'(b_x \hat{x} + b_y \hat{y} + b_z \hat{z}), \tag{26}$$

where

$$b_x = (\mathbf{N}_e)^2 (n_e^2 - c_{xx}^{(e)}) - n_e^2 (N_{yz}^e)^2, \tag{27}$$

$$b_y = -(\mathbf{N}_e)^2 c_{xy}^{(e)} - n_e^2 N_{yz}^e N_{zx}^e, \tag{28}$$

$$b_z = -(\mathbf{N}_e)^2 c_{xz}^{(e)} - n_e^2 N_{yz}^e N_{xy}^e, \tag{29}$$

and the proportionality coefficient in Eq. (26) may be chosen as $(b_x^2 + b_y^2 + b_z^2)^{-1/2}$, which makes **e**, as well as **o**, a unit vector.

After determining the directions **o** and **e**, the whole vector of the electric field in the lowest (zero) order of the λ expansion (2) can be presented as

$$\mathbf{E}^{(0)}(\mathbf{r}) = E_o \mathbf{o} e^{ik_0 S_o} + E_e \mathbf{e} e^{ik_0 S_e}. \tag{30}$$

In this expression, E_o and E_e are the complex electric field amplitudes of the ordinary and extraordinary waves. To find these amplitudes, higher (than the lowest) order terms in the λ expansion, as given by Eq. (2), must be considered. In general, fields of higher than the lowest order will not be a simple linear combination of **o** and **e**, as in Eq. (30). This is already clear from the following consideration. After substituting Eq. (30) into Eq. (1) and taking into account that Eq. (1) is a vector equation, we have three differential equations to determine only two amplitudes E_o and E_e (which is impossible in the general case). To remove this discrepancy, it is enough to add a third term to the linear combination in Eq. (30). This term must be proportional to some vector **s**, and this vector must be linearly independent of **o** and **e**, but otherwise arbitrary. For mathematical convenience (see later), the vector **s** in this study was chosen as

$$\mathbf{s} = \frac{\boldsymbol{\nabla}(S_o + S_e)}{|\boldsymbol{\nabla}(S_o + S_e)|}, \tag{31}$$

and the whole vector of the electric field in the first order approximation can be presented as

$$\mathbf{E}^{(1)}(\mathbf{r}) = E_o \mathbf{o} e^{ik_0 S_o} + E_e \mathbf{e} e^{ik_0 S_e} + \frac{E_s \mathbf{s}}{ik_0} e^{ik_0 (S_o + S_e)/2}. \tag{32}$$

From a physical point of view the last term in Eq. (32) provides the coupling between ordinary and extraordinary waves in this method of describing wave propagation in anisotropic media. As has already been mentioned in the Introduction, this term is important in regions (like a wall defect or near-substrate regions) where the characteristic anisotropy strength ν can be of order $1/k_0 l$ (in these regions the characteristic scale of the medium inhomogeneity l is of the order of the correlation length ξ and is relatively small at high voltages). Substituting this expression into the time-harmonic wave equation and combining terms with the first power of ik_0, one can derive equations for the amplitudes E_o, E_e, and E_s. It is worth mentioning, again, that the lowest $[(ik_0)^2]$ order terms will vanish identically, because $\mathbf{o}, S_o$ and $\mathbf{e}, S_e$ satisfy Eq. (3).

Using this set of vectors (**o**,**e**,**s**) as a basis, the general λ expansion

$$\mathbf{E}(\mathbf{r}) = e^{ik_0 (S_o + S_e)/2} \sum_{m=0}^{\infty} \frac{1}{(ik_0)^m} \times [O_m \mathbf{o} e^{-ik_0 \Delta S(\mathbf{r})} + E_m \mathbf{e} e^{ik_0 \Delta S(\mathbf{r})} + Z_m \mathbf{s}] \tag{33}$$

can also be used to determine higher order corrections to the first order approach for the amplitudes by substituting Eq. (33) into the wave equation (1). In Eq. (33)

$$\Delta S(\mathbf{r}) = \frac{1}{2}[S_e(\mathbf{r}) - S_o(\mathbf{r})]. \tag{34}$$

It is clear also that $O_0 \equiv E_o$, $E_0 \equiv E_e$, $Z_1 \equiv E_s$, and $Z_0 = 0$. Combining terms with equal powers of $(1/ik_0)$ in Eq. (1), one can derive equations for $O_m(\mathbf{r})$, $E_m(\mathbf{r})$, and $Z_m(\mathbf{r})$ in each order in the λ expansion. In principle, these equations can be solved numerically using the known results for the lower order amplitude calculations.

In this study only the lowest order approximation for the complex amplitudes was used. Substituting expression (32) in Eq. (1), one finds the following resulting equations for $E_o(\mathbf{r})$, $E_e(\mathbf{r})$, and $E_s(\mathbf{r})$:

$$e_- G_{ik}^o (E_o o_k) + e_+ G_{ik}^e (E_e e_k) = E_s A_i. \tag{35}$$

In these equations $e_\pm \equiv \exp(\pm ik_0 \Delta S)$, $i = 1,2,3$,

$$G_{ik}^o (E_o o_k) = 2\partial_k S_o \partial_k (E_o o_i) - \partial_i S_o \partial_k (E_o o_k) - \partial_k S_o \partial_i (E_o o_k), \tag{36}$$

$$\begin{aligned} G_{ik}^e (E_e e_k) = {} & 2\partial_k S_e \partial_k (E_e e_i) + \partial_k [\partial_k S_e (E_e e_i)] \\ & - \partial_i [\partial_k S_e (E_e e_k)] - \partial_k S_e \partial_k (E_e e_i) \\ & - \partial_i S_e \partial_k (E_e e_k), \end{aligned} \tag{37}$$

$$A_i = \epsilon_{ik s_k}, \quad \partial_k F \equiv \frac{\partial F}{\partial x_k}, \tag{38}$$

and, again, summing over repeated indices is assumed. Equations (35) do not contain space derivatives of the amplitude E_s. This is a consequence of the specific choice of vector **s** in Eq. (31) and the identity $\nabla^2 \mathbf{E} - \boldsymbol{\nabla}(\boldsymbol{\nabla} \cdot \mathbf{E}) = \boldsymbol{\nabla} \times (\boldsymbol{\nabla} \times \mathbf{E})$. Eliminating E_s from Eqs. (35) gives a final set of two first order differential equations for the unknown complex amplitudes E_o and E_e of the ordinary and extraordinary waves:

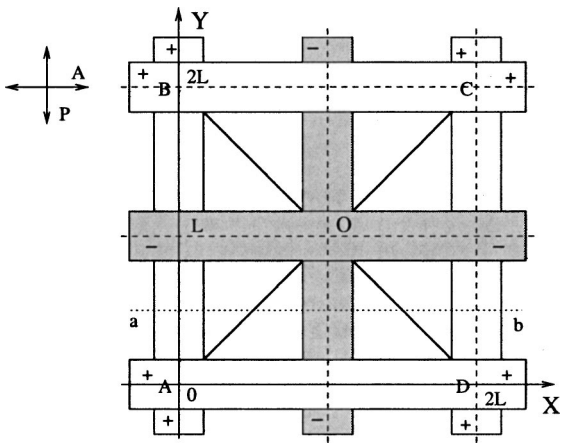

FIG. 1. Top view of the HMD cell. The cell possesses $2L$ periodicity along both the x and y directions. The orientation of the crossed analyzer and polarizer is shown in the upper left corner.

$$A_z[e_- G^o_{xk}(E_o o_k)+e_+ G^e_{xk}(E_e e_k)] = A_x[e_- G^o_{zk}(E_o o_k)+e_+ G^e_{zk}(E_e e_k)] \tag{39}$$

and

$$A_z[e_- G^o_{yk}(E_o o_k)+e_+ G^e_{yk}(E_e e_k)] = A_y[e_- G^o_{zk}(E_o o_k)+e_+ G^e_{zk}(E_e e_k)]. \tag{40}$$

These equations can be solved numerically using appropriate boundary conditions (see the example in the next section).

One important remark can be made in concluding this section. We have described the GOA formalism in the case when the optical properties (director) depend on all three space coordinates. In the case when $\hat{\mathbf{n}}$ (and, hence, $\hat{\boldsymbol{\epsilon}}$) depends on only two coordinates, say, x and z, the following simplifications are possible. First, in Eqs. (8)–(16) for the extraordinary eikonal, one can substitute $S_e \rightarrow n_{gy} y + S_e(x,z)$, where $n_{gy}=k_{gy}/k_0$ and k_{gy} is the y component of the wave vector in the isotropic medium adjacent to the liquid crystal film. Equation (16) will be the same, with the substitution $\partial S_e/\partial y \rightarrow n_{gy}$ in the coefficients B and C. Finally, because E_o, E_e, $\mathbf{o}$, and $\mathbf{e}$ do not depend on the y coordinate, one can drop the y derivatives of $E_o\mathbf{o}$ and $E_e\mathbf{e}$ in Eqs. (35)–(37) [and then in Eqs. (39) and (40)].

III. APPLICATION OF THE GOA TO A LIQUID CRYSTAL CELL WITH THREE-DIMENSIONAL DIRECTOR VARIATIONS

In this section the GOA is applied to calculation of the light transmittance of a cell exhibiting the homeotropic to multidomainlike transition (HMD cell) [29]. As was shown in [30], due to the symmetries of the cell, it is enough to calculate the director in the volume inside the right triangular prism with the triangle OCD as its horizontal cross section, as shown in Fig. 1, and then extend the results to the rest of the cell using symmetry. However, in the general case of oblique incidence of a plane wave, the transmitted electromagnetic field violates all the symmetries of the cell except periodicity in the x and y directions. Thus, the light transmittance calculation needs to consider the whole volume inside the right square $2L\times 2L$ prism which is shown schematically in Fig. 1. It is assumed that a plane wave comes through air from beneath the cell, and passes through the entrance polarizer, the first glass substrate, the liquid crystal film, the second glass substrate, and finally the analyzer. In all the results of light transmittance calculations presented here, the polarizer and analyzer were considered as ideal (having thickness of several micrometers), and transmittance losses in two air-polarizer interfaces were taken into account.

To solve the eikonal equations (7) and (16) and the amplitude equations (39) and (40), corresponding boundary conditions for S_o, S_e, E_o, and E_e must be specified. In the case of a plane wave incident on a planar liquid crystal layer from an isotropic glass medium, the kinematic boundary conditions, first of all, must be satisfied along the glass-liquid crystal interface:

$$\frac{\partial S_i}{\partial x}=n_{gx}, \quad \frac{\partial S_i}{\partial y}=n_{gy}, \quad i=o,e, \tag{41}$$

where $\mathbf{n}_g=\mathbf{k}_g/k_0=(n_{gx},n_{gy},n_{gz})$, where $\mathbf{k}_g$ is the wave vector in the glass. The $2L$ periodicity along both x and y directions gives the other pair of conditions that must be satisfied by Eqs. (7) and (16):

$$S_i(x+2L,y,z)=S_i(x,y,z)+2Ln_{gx}, \tag{42}$$

$$S_i(x,y+2L,z)=S_i(x,y,z)+2Ln_{gy}. \tag{43}$$

Using these boundary and quasiperiodicity conditions, the eikonal equation (7) for the ordinary wave can be solved analytically. The result is

$$S_o(x,y,z)=n_{gx}x+n_{gy}y+n_{oz}z,$$

where

$$n_{oz}=\sqrt{n_o^2-n_{gx}^2-n_{gy}^2}. \tag{44}$$

In general, the eikonal equation (16) must be solved numerically for the extraordinary wave. In this study the centered finite difference method implicit in the z direction was used, and the resulting nonlinear system of algebraic equations was solved using the nonlinear Gauss-Seidel method.

Similar periodicity conditions must be satisfied for the ordinary E_o and extraordinary E_e amplitudes:

$$E_i(x+2L,y,z)=E_i(x,y,z), \tag{45}$$

$$E_i(x,y+2L,z)=E_i(x,y,z), \tag{46}$$

where $i=o,e$. The other boundary conditions for E_o and E_e come from the continuity property of the tangential components of the electric and magnetic fields along the glass-liquid crystal interface:

$$\mathbf{E}_{gt}+\mathbf{E}''_{gt}=\mathbf{E}'_t, \quad \mathbf{H}_{gt}+\mathbf{H}''_{gt}=\mathbf{H}'_t, \tag{47}$$

where the tangential components of the electric $\mathbf{E}_{gt}, \mathbf{E}''_{gt}$ and magnetic $\mathbf{H}_{gt}, \mathbf{H}''_{gt}$ fields correspond to incident and reflected electromagnetic waves in the isotropic glass medium adjacent to the interface, and $\mathbf{E}'_t, \mathbf{H}'_t$ describe the transmitted electromagnetic field in the layer of liquid crystal adjacent to the interface. In accordance with [29], strong homeotropic anchoring on both glass substrates can be assumed. This means that the first liquid crystal layer adjacent to the glass-liquid crystal interface is homeotropic and described by a diagonal dielectric tensor ϵ_{ik} with $\hat{\mathbf{n}} = \pm \hat{z}$ in Eq. (5). Thus, application of the formulas (47) gives the following boundary conditions for the amplitudes of the ordinary E_o and extraordinary E_e waves:

$$E_o = \frac{2n_{gz}E_{gy'}}{n_{0z}+n_{gz}}, \quad E_e = \frac{2n_g^2 n_{gz}E_{gx'}}{n_g^2 n_{0z}+n_o^2 n_{gz}}. \tag{48}$$

In these expressions $E_{gx'}$ and $E_{gy'}$ are the corresponding components of the electric field at the glass side of the glass-liquid crystal interface. They are calculated in the incidence coordinate system (x',y',z) produced by rotating the laboratory system (x,y,z) (shown in Fig. 1) by the angle ϕ_a around the z axis, where ϕ_a is the azimuthal angle of the incident plane. Then,

$$n_{oz} = \sqrt{n_o^2 - \sin^2\theta_a}, \quad n_{gz} = \sqrt{n_g^2 - \sin^2\theta_a} \tag{49}$$

where n_g is the refraction index in the glass and θ_a is the incidence polar angle in air. Taking into account the periodicity conditions (45) and (46) and boundary conditions (48), Eqs. (39) and (40) were solved numerically inside the liquid crystal cell using the implicit finite difference method.

After passing the liquid crystal cell, the calculated electromagnetic field $\mathbf{E} \equiv \mathbf{E}^{(1)}$ will be a complicated function of the x and y coordinates. It is convenient to extract the factor $\exp(ik_0 S_o)$ from this function and expand the rest in a double Fourier series using $2L$ periodicity in both x and y directions. Thus, at the beginning of the second glass substrate,

$$\mathbf{E} = e^{ik_0 S_o}\mathbf{E}_f(x,y) = e^{ik_0 S_o}\sum_{p,q} \mathbf{E}_{pq} e^{ik_L(px+qy)}, \quad k_L \equiv \frac{\pi}{L}. \tag{50}$$

Solving the time-harmonic wave equation $\nabla^2\mathbf{E} = -(k_0 n_g)^2\mathbf{E}$ in the homogeneous and isotropic glass medium with the initial conditions (50) and taking into account only transmitted waves, the resulting expression for $\mathbf{E}$ in the second glass substrate can be represented as a plane-wave expansion,

$$\mathbf{E} = e^{ik_0 S_o}\mathbf{E}_f(x,y) = e^{ik_0 S_o}\sum_{p,q} \mathbf{E}_{pq} e^{ik_L(px+qy)} e^{ik_0 n_{pq} z}, \tag{51}$$

where

$$n_{pq} = \sqrt{n_g^2 - (n_{ax}+c_L p)^2 - (n_{ay}+c_L q)^2} \tag{52}$$

with $c_L = \lambda/2L$, $n_{ax} = \sin\theta_a \cos\phi_a$, and $n_{ax} = \sin\theta_a \sin\phi_a$.

Thus, the electromagnetic field in the second glass substrate can be represented as a wave packet of plane waves (51) with known amplitudes $\mathbf{E}_{pq}$ and wave vectors

$$\mathbf{k}_{gpq} = k_0[(n_{ax}+c_L p),(n_{ay}+c_L q),n_{pq}]. \tag{53}$$

It is worth noticing that $(n_{ax}+c_L p)^2 + (n_{ay}+c_L q)^2$ cannot exceed 1 (which is equivalent to the total internal reflection of all waves with sufficiently large x and y components of their wave vectors from the analyzer-air interface). This means that we do not have to consider waves with numbers p and q lying outside the circle

$$(p+R_g n_{ax})^2 + (q+R_g n_{ay})^2 = R_g^2 \tag{54}$$

of radius $R_g = 1/c_L = 2L/\lambda$ in the (p, q) plane. For $2L = 60\ \mu$m, the total number of Fourier harmonics N_{pq} is about 85 000. However, calculations show that a much smaller number is enough to produce stable results. If, for example, one considers only waves with $|p| \leqslant 20$ and $|q| \leqslant 20$, the addition of the other Fourier harmonics does not change the result for light transmittance significantly. In the case of a cell with a reduced size of $2L = 20\ \mu$m, N_{pq} is about 4200, and limitation (54) is more important. In this study the contribution of all N_{pq} waves to the light transmittance was taken into account in the case of the reduced size cell.

The resulting amplitude of the electric field in air $\mathbf{E}^a$ can be represented as the following superposition of the results $\mathbf{E}^a_{pq}$ of transmittance of each wave through the analyzer:

$$\mathbf{E}^a = \sum_{p,q} \mathbf{E}^a_{pq} e^{ig_{pq}} e^{ik_L(px+qy)}, \tag{55}$$

where $g_{pq} = d_g k_0 n_{pq}$. In this expression the phase factor $\exp(ig_{pq})$ arises after passing the second glass substrate. Because n_{pq} depends on the p and q numbers of a particular plane wave, the corresponding differential light transmittance $T(x,y) \sim \mathbf{E}(x,y)\cdot\mathbf{E}^*(x,y)$ also depends on d_g. However, because $|e^{ig_{pq}}| = 1$, the light transmittance T_{av} produced by averaging $T(x,y)$ over the square $2L \times 2L$ does not depend on the glass thickness.

The results of application of the GOA to the HMD cell are shown in Figs. 2–11 for the case of normal incidence, when light is traveling from beneath the cell. All the results presented in these figures are produced for the orientation of the crossed polarizer and analyzer shown in Fig. 1. The results of the optical path difference calculations shown in Fig. 2 and the results of the differential light transmittance calculations shown in Figs. 3–5, 7, and 10 were produced along the line *ab* (see Fig. 1). The electrodes were considered as transparent, and we assumed that $n_o = n_g = 1.5$ and $\lambda = 0.55\ \mu$m. We use the director patterns for this liquid crystal cell produced in Refs. [30] and [31] using two methods: a simplified model and direct computer calculation. It will be shown that both methods lead to essentially the same optics results. Figures 2–9 describe the HMD cell with geometrical sizes used in the experiment [29]: $2L = 60\ \mu$m, electrode width $l = 10\ \mu$m, and $d = 5\ \mu$m. The liquid crystal material chosen

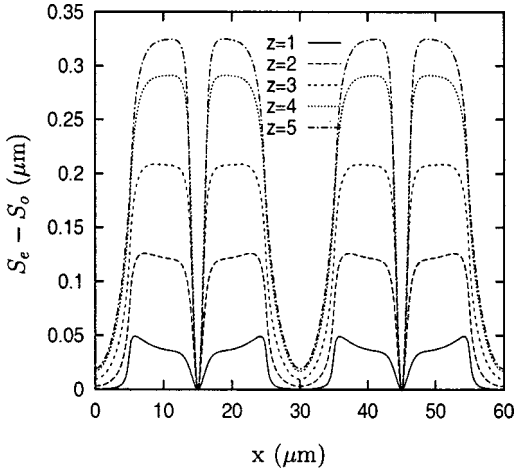

FIG. 2. Optical path difference distributions at different values of the z coordinate (in μm) and at $u=18$ V.

in the experimental cell possesses the birefringence $\Delta n \equiv n_e - n_o = 0.088$. The other figures are plotted for the same type of cell but with three times smaller sizes in the x and y directions: in Figs. 10 and 11 $2L=20$ μm, $l=3.33$ μm, and $d=5$ μm.

Figure 2 illustrates the evolution of the optical path difference $S_e - S_o$ for different values of the z coordinate ($z=0$ corresponds to the bottom and $z=d=5$ μm to the top of the liquid crystal film). Minima at $x=15$ and 45 μm correspond to the wall defect regions where the director distribution is close to homeotropic and the optical path difference at the exit of the liquid crystal film is small. As was shown in Ref. [30], the director distribution is also close to homeotropic in the electrode regions (near the points $x=0$, 30, and 60 μm in Fig. 2), and $S_e - S_o$ at the top substrate is also small. Throughout the rest of the cell the director distribution is close to planar [30] and the optical path difference is large.

Figure 3 displays the dependence of $T(x,y)$ on d_g. As has already been mentioned, $T_{\rm av}$ does not depend on d_g, and changing the glass thickness leads only to a redistribution of the differential light transmittance throughout the (x,y) plane. In all further figures an artificially small value of d_g

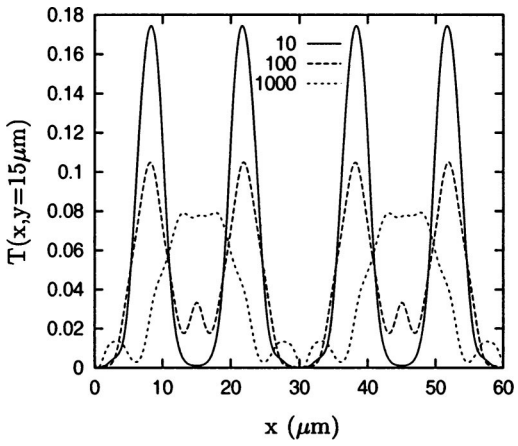

FIG. 3. Distribution of the differential light transmittance for different glass thicknesses: $d_g=10$, 100, and 1000 μm; $u=10$ V.

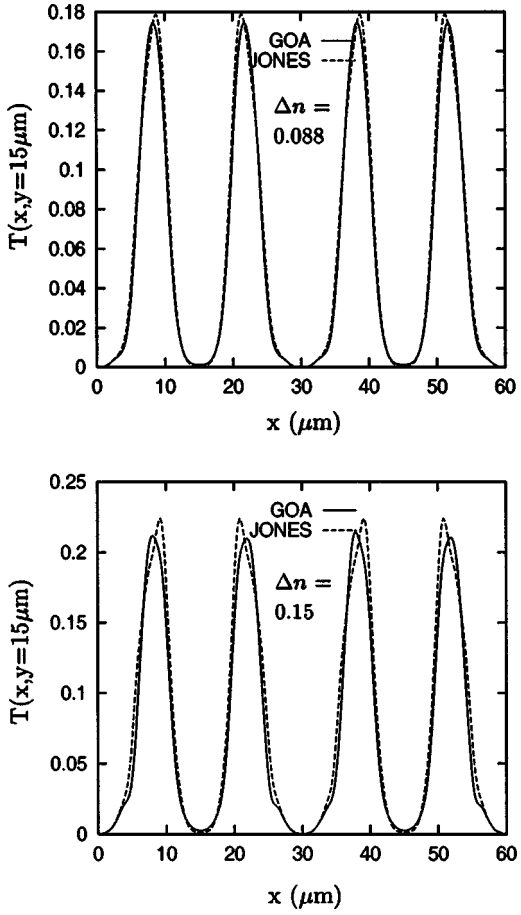

FIG. 4. Differential light transmittance for $u=10$ V. The value of Δn is 0.088 in the upper graph and 0.15 in the lower one.

$=10$ μm was chosen. The reason is that for this (or smaller) value of d_g, the influence of the glass layer on the differential light transmittance is relatively small, and $T(x,y)$ reflects mostly properties of the director distribution.

Figures 4 and 5 illustrate the dependence of the spatial distribution of the differential light transmittance $T(x,y)$ on voltage u and birefringence Δn. Each figure provides also a comparison between the GOA and the Jones calculus method for different values of u and Δn. As one finds, the differential light transmittance is small in the wall defect and electrode regions in accordance with the results of the optical path calculations shown in Fig. 2. As follows also from these figures, the difference in $T(x,y)$ between the GOA and Jones calculus increases when u and Δn increase. This is expected, because for larger u we have sharper director variations in the x and y directions, and the corresponding spatial derivatives (which are ignored in the Jones model) become increasingly important. It is also clear that for larger Δn the influence of these sharp changes of the director on optical properties is more tangible. The calculation of the averaged light transmittance $T_{\rm av}$ is in accordance with these observation as well. Figure 6 displays $T_{\rm av}$ as given by the GOA and Jones calculus models. It shows that the two methods produce very similar results for small values of the birefringence, but the difference increases with Δn. It is worth mentioning that the structure of the wall defect region of the

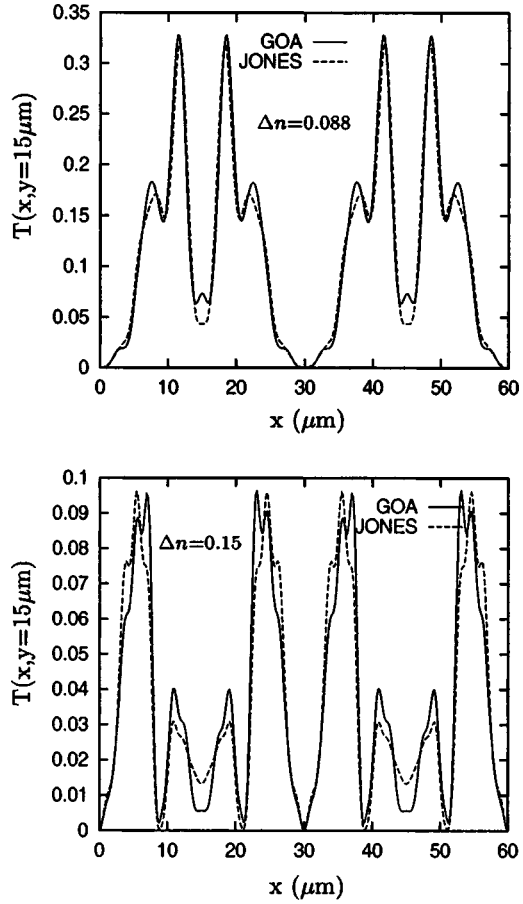

FIG. 5. Differential light transmittance for $u=18$ V. The value of Δn is 0.088 in the upper graph and 0.15 in the lower one.

HMD cell differs from the one in the 2D cell, which combines the concept of in-plane switching with vertical alignment [24,32]. In the 2D case the surfaces where the director stays homeotropic when u is nonzero are planes. However, the corresponding surfaces in the HMD cell, as was found in [30], are more complicated. They are close to diagonal planes of the cell [like the planes *AC* and *BD* in Fig. 1 which go perpendicular to the (x,y) plane along the lines *AC* and *BD*] only for values of the z coordinate close to the midpoint between the substrates and deviate significantly from these diagonal planes in the near-substrate regions. Because of this feature, the effect of ray focusing in the HMD cell is less pronounced than in the 2D cell.

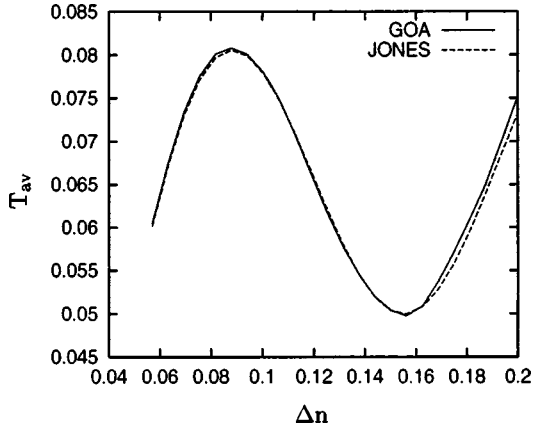

FIG. 6. Δn dependence of the averaged light transmittance for the GOA and the Jones calculus at $u=18$ V.

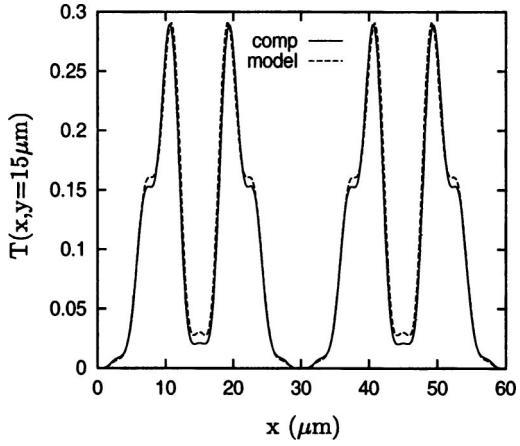

FIG. 7. Differential light transmittance for the model and direct computer calculation $u=12$ V and $\Delta n=0.088$.

Figure 7 displays $T(x,y)$ for the director patterns calculated in two ways: using the model proposed in Refs. [30–32] and direct computer calculation at $u=12$ V and $\Delta n=0.088$. The main idea of the model is to numerically solve the dynamic equation $\gamma_1 \partial_t \hat{\mathbf{n}} = -\delta F/\delta \hat{\mathbf{n}}$ for the director using a corresponding exact expression for the free energy F but an approximate analytical expression for the electric field $\mathbf{E}$. In contrast, the previously used methods of direct computer solution (e.g., the relaxation method) do not use an approximate form for the electric field but instead solve $\boldsymbol{\nabla}\cdot\mathbf{D}=0$ to get the electric field after each director update, based on the dynamic equation. As was shown in Refs. [30] and [32], the proposed model helps to understand better the director and electric field behavior in liquid crystal cells and is much faster than direct computer calculation, giving essentially the same results for the director distribution. Figure 7 shows a good agreement in $T(x,y)$ between the model and direct computer calculation, which can serve as additional confirmation of the accuracy of the model. Figure 8 shows the voltage-dependent T_{av} (*TV* curve) for the voltage range that is relevant for display applications. The agreement between the model and direct computer calculation is good.

Figure 9 illustrates the voltage dependence of T_{av} for different values of Δn using the GOA. When Δn is relatively small ($\Delta n \approx 0.06$ or smaller), the corresponding *TV* curve increases monotonically, reaching its asymptotic value, which corresponds to the director pattern, at $u=\infty$. For larger birefringence, a maximum on the *TV* curve appears at some $u=u^*$. When Δn increases further, $T_{\mathrm{av}}(u^*)$ and u^* decrease. After passing the maximum ($u>u^*$), the light transmittance decreases with increasing voltage and finally approaches its asymptotic value $T_{\mathrm{av}}(u=\infty)<T_{\mathrm{av}}(u^*)$. This type of voltage dependence of T_{av} can easily be explained qualitatively. For a large Δn, even a relatively small average deviation of the director $\hat{\mathbf{n}}$ from its homeotropic distribution $\hat{\mathbf{n}}=\pm\hat{\mathbf{z}}$ (at some small voltage) produces the optical path

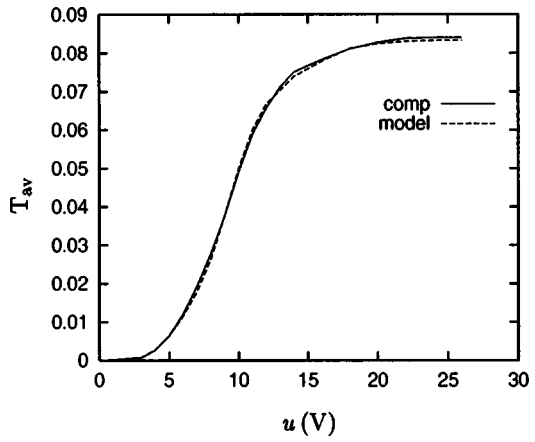

FIG. 8. Averaged light transmittance vs voltage (*TV* curve). The solid curve is calculated using the model and the dashed curve is obtained from direct computer calculation.

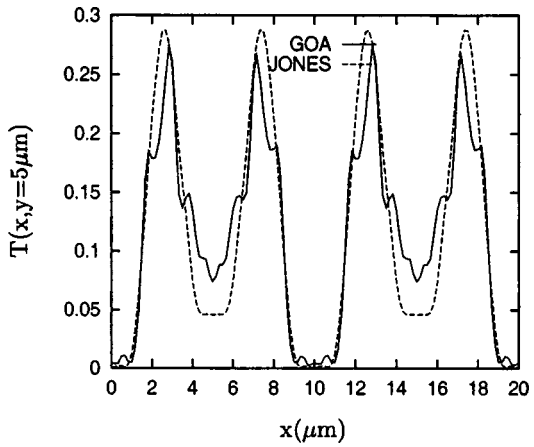

FIG. 10. Differential light transmittance for the GOA and the Jones calculus models for the HMD cell with reduced sizes; $u=10$ V, $\Delta n=0.088$.

difference S_e-S_o which corresponds to the final orientation of the polarization of the outcoming radiation along the transmittance axis of the analyzer. In this case the light transmittance is maximum. A larger deviation of $\hat{\mathbf{n}}$ from $\hat{\mathbf{n}}=\pm\hat{z}$ rotates the polarization plane further, and the light transmittance decreases.

Figure 10 presents $T(x,y)$ in both the GOA and the Jones calculus models but for smaller geometrical sizes of the HMD cell: period $2L=20\ \mu$m and the electrode width $l=3.33\ \mu$m ($d=5\ \mu$m is the same). Clearly, the difference between the GOA and Jones calculus models in this case is more significant than for the cell with larger sizes (compare with Fig. 4). Finally, Fig. 11 compares *TV* curves produced by the GOA and Jones calculus models also for the cell with reduced sizes. It shows that for $u>8$ V the difference between the two methods is significant (which is in accordance with Fig. 10). The difference between the GOA and Jones calculus results for T_{av} in the case of the experimental cell is very small for the voltage range $u\leqslant 25$ V. (It is not shown here because the difference is so small.) A qualitative explanation of these last results is as follows. There are two regions of lateral director variations. The first one corresponds to the wall defect area. In this region the characteristic distance of the director variation l is of the order of the electric relaxation length ξ. For high voltage ξ may be comparable with λ, and even the results of the GOA for $T(\mathbf{r})$ across this region may be only qualitatively correct. However, because the volume of the wall defect region is relatively small, its contribution to T_{av} is also small. In the second region (the rest of the cell) l is of the order of the corresponding geometrical sizes of the cell. For this cell $l=l_{el}$ (where l_{el} is the electrode width) may be chosen. Even in the case of the reduced geometrical sizes of the cell considered here, l_{el} is of order of several micrometers, $1/k_0 l_{el}\ll 1$, and the GOA is still applicable. It is clear, however, that for the reduced cell the x and y derivatives become more important. For this reason the difference in results between the GOA and Jones calculus methods increases with decreasing $2L$ and l_{el}, because the latter model completely ignores these derivatives, and the Jones calculus method becomes questionable. In such a situation, taking into account also that the calculational times in both the GOA and Jones calculus methods are comparable (and much smaller than in the case of the FDTD method), the GOA is preferable.

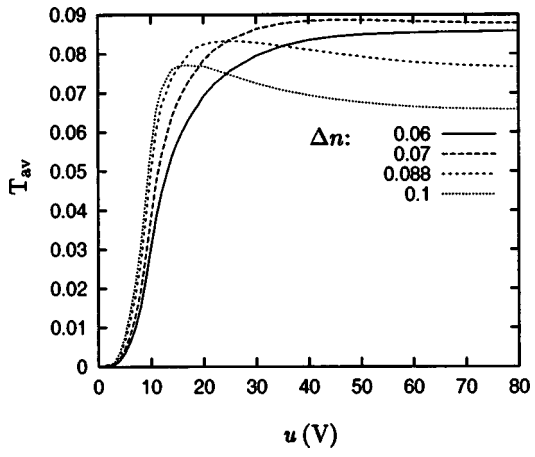

FIG. 9. *TV* curves for different values of the birefringence Δn.

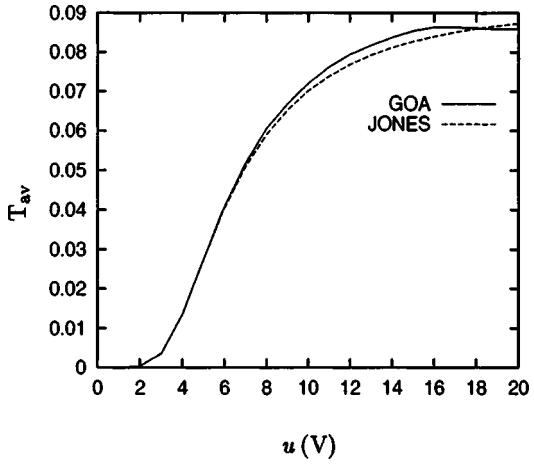

FIG. 11. Averaged light transmittance vs voltage (*TV* curve) for the HMD cell with reduced sizes and $\Delta n=0.088$.

IV. CONCLUSIONS

The geometrical optics approach has been applied to the calculation of the differential and averaged light transmittance for the case of a liquid crystal film whose director varies in three spatial dimensions. A liquid crystal cell that exhibits the homeotropic to multidomainlike transition was considered as an example of the GOA application. The GOA provides a fast method of calculating the light transmittance (almost as fast as the Jones calculus method), giving a more accurate description than the Jones calculus results for a liquid crystal cell whose director variations occur on the micrometer scale and comparable results for cells with variations on larger length scales. The GOA is especially useful for a 3D cell when the finite difference time domain method is extremely time consuming.

ACKNOWLEDGMENT

This work was supported in part by National Science Foundation Grant No. DMS-0107761.

[1] D. W. Berreman, J. Opt. Soc. Am. **63**, 1374 (1973).
[2] A. Lien, Liq. Cryst. **22**, 171 (1997).
[3] J. Anderson, P. Bos, C. Cai, and A. Lien, Soc. Inf. Display Int. Symp. Dig. **30**, 628 (1999).
[4] B. Witzigmann, P. Regli, and W. Fichtner, J. Opt. Soc. Am. A **15**, 753 (1998).
[5] C. Titus, P. Bos, and J. Kelly, Soc. Inf. Display Int. Symp. Dig. **30**, 624 (1999).
[6] E. E. Kriezis and S. J. Elston, Opt. Commun. **165**, 99 (1999).
[7] A. Taflove and S. C. Hagness, *Computational Electrodynamics: The Finite-Difference Time-Domain Method* (Artech, New York, 2000).
[8] C. V. Brown and E. E. Kriezis, J. Appl. Phys. **91**, 3495 (2002).
[9] E. E. Kriezis and S. J. Elston, J. Mod. Opt. **46**, 1201 (1999).
[10] E. E. Kriezis and S. J. Elston, Liq. Cryst. **26**, 1663 (1999).
[11] E. E. Kriezis and S. J. Elston, Appl. Opt. **39**, 5707 (2000).
[12] Y. A. Kravtsov and Y. I. Orlov, *Geometrical Optics of Inhomogeneous Media* (Springer-Verlag, New York, 1990).
[13] R. Courant and P. D. Lax, Proc. Natl. Acad. Sci. U.S.A. **42**, 872 (1956).
[14] R. Courant, *Partial Differential Equations* (Interscience, New York, 1962).
[15] Y. A. Kravtsov, Dokl. Akad. Nauk SSSR **183**, 74 (1968).
[16] A. A. Fuki, Y. A. Kravtsov, and O. N. Naida, *Geometrical Optics of Weakly Anisotropic Media* (Gordon and Breach, New York, 1998).
[17] H. L. Ong and R. B. Meyer, J. Opt. Soc. Am. **73**, 167 (1983).
[18] H. L. Ong and R. B. Meyer, J. Opt. Soc. Am. A **2**, 198 (1985).
[19] H. L. Ong, Appl. Phys. Lett. **51**, 1398 (1987).
[20] H. L. Ong, J. Appl. Phys. **64**, 4867 (1988).
[21] J. A. Kosmopoulos and H. M. Zenginoglou, Appl. Opt. **26**, 1714 (1987).
[22] H. M. Zenginoglou and J. A. Kosmopoulos, Appl. Opt. **28**, 3516 (1989).
[23] J. A. Reyes, Phys. Rev. E **57**, 6700 (1998).
[24] W. Liu, J. Kelly, and J. Chen, Jpn. J. Appl. Phys., Part 1 **38**, 2779 (1999).
[25] K. H. Kim, S. B. Park, J. U. Shim, J. Chen, and J. H. Souk, in *Proceedings of the Fourth International Display Workshops (IDW '97), Nagoya, Japan, 1997* (Society for Information Display, San Jose, CA, 1997), Vol. 1, p. 175.
[26] S. H. Lee, H. Y. Kim, T. K. Jung, I. C. Park, Y. H. Lee, B. G. Rho, J. S. Park, and H. S. Park, in *Proceedings of the Fourth International Display Workshops* [25], Vol. 1, p. 9.
[27] W. Liu and J. Kelly, Mol. Cryst. Liq. Cryst. Sci. Technol., Sect. A **359**, 647 (2001).
[28] L. D. Landau and E. M. Lifshitz, *Electrodynamics of Continuous Media* (Pergamon, New York, 1960).
[29] S. H. Lee, H. Y. Kim, Y. H. Lee, I. C. Park, B. G. Rho, H. G. Galabova, and D. W. Allender, Appl. Phys. Lett. **73**, 470 (1997).
[30] G. Panasyuk and D. W. Allender, J. Appl. Phys. **91**, 9603 (2002).
[31] G. Panasyuk, D. W. Allender, and J. Kelly, Soc. Inf. Display Int. Symp. Dig. **32**, 850 (2001).
[32] G. Panasyuk, D. W. Allender, and J. Kelly, J. Appl. Phys. **89**, 4777 (2001).